

Three Dimensional Combined Fracture-Plastic Material Model for Concrete including Creep and Rate Effect for dynamic Loading

Jan Červenka and Vladimír Červenka

ČERVENKA CONSULTING, Předvoje 22, 162 00, Prague 6, Czech Republic

E-mail: cervenka@cervenka.cz, WWW: <http://www.cervenka.cz>

The research work was supported by Czech Grant Agency under contract

Nr. 103/99/0755

Summary:

This paper describes a combined fracture-plastic model. The fracture model is based on the classical orthotropic smeared crack formulation and crack band model. It employs Rankine failure criterion, exponential softening, and it can be used as rotated or fixed crack model. The hardening/softening plasticity model is based on Menétrey-Willam or Drucker-Prager failure surface. Both models use return mapping algorithm for the integration of constitutive equations. Special attention is given to the development of an algorithm for the combination of the two models. The presented combined algorithm is based on recursive substitution, and it allows for the two models to be developed and formulated separately. The algorithm can handle cases when failure surfaces of both models are active, but also when physical changes such as crack closure occur. The model can be used to simulate concrete cracking, crushing under high confinement, and crack closure due to crushing in other material directions.

Keywords: fracture mechanics, plasticity, smeared crack model, concrete, finite element method.

1. Introduction

This paper covers the description of a three-dimensional constitutive material model for concrete, which combines plasticity with fracture. Fracture is modeled by an orthotropic smeared crack model based on Rankine tensile criterion. Hardening/softening plasticity model based on Menétrey-Willam [1] three-parameter failure surface is used to model concrete crushing. Although many papers have been published on plasticity models for concrete (for instance [2,3,4,5,6]) or smeared crack models ([7,8,9,10,11]), there are not many description of their successful combination in the literature. Owen et al. [12] presented a combination of cracking and viscoplasticity. Comprehensive treatise of the problem was provided also by de Borst [10], and recently several works have been published on the combination of damage and plasticity (Simo and Ju [13], Meschke et al. [14]). The presented model differs from the above formulations by ability to handle also physical changes like for instance crack closure, and it is not restricted to any particular shape of hardening/softening laws. Also within the proposed approach it is possible to formulate the two models (i.e. plastic and fracture) entirely separately, and their combination can be provided in a different algorithm or model. From programming point of view such approach is well suited for object oriented programming.

The method of strain decomposition as it was introduced by de Borst [10] is used to combine fracture and plasticity models together. Both models are developed within the framework of return mapping algorithm (Wilkins [15]). This approach guarantees the

solution for all magnitudes of strain increment. From an algorithmic point of view the problem is then transformed into finding an optimal return point on the failure surface.

The combined algorithm must determine the separation of strains into plastic and fracturing components, while it must preserve the stress equivalence in both models.

The proposed algorithm is based on a recursive iterative scheme. It can be shown that such a recursive algorithm cannot reach convergence in certain cases such as, for instance, softening and dilating materials. For this reason the recursive algorithm is extended by a variation of the relaxation method to stabilize convergence.

In the first part of the paper, the formulation of the fracture and plastic model respectively is provided. This part also contains a description of the recursive algorithm for the combination of the two material models. The numerical behavior of this algorithm is demonstrated under several selected loading histories in the subsequent section. The last section demonstrates the model performance in practical engineering applications, and it contains a comparison with experimental results.

2. Material model formulation

The material model formulation is based on the strain decomposition into elastic ε_{ij}^e , plastic ε_{ij}^p and fracturing ε_{ij}^f components (de Borst [10]).

$$\varepsilon_{ij} = \varepsilon_{ij}^e + \varepsilon_{ij}^p + \varepsilon_{ij}^f \quad (1)$$

The new stress state is then computed by the formula:

$$\sigma_{ij}^n = \sigma_{ij}^{n-1} + E_{ijkl}(\Delta\varepsilon_{kl} - \Delta\varepsilon_{kl}^p - \Delta\varepsilon_{kl}^f) \quad (2)$$

where the increments of plastic strain $\Delta\varepsilon_{ij}^p$ and fracturing strain $\Delta\varepsilon_{ij}^f$ must be evaluated based on the used material models.

2.1 Rankine-fracturing model for concrete cracking

Rankine criterion is used for concrete cracking

$$F_i^f = \sigma_{ii}' - f_{ti}' \leq 0 \quad (3)$$

It is assumed that strains and stresses are converted into the material directions, which in case of rotated crack model correspond to the principal directions, and in case of fixed crack model, are given by the principal directions at the onset of cracking.

Therefore, σ_{ii}' identifies the trial stress and f_{ti}' tensile strength in the material direction \square . Prime symbol denotes quantities in the material directions. The trial stress state is computed by the elastic predictor.

$$\sigma_{ij}' = \sigma_{ij}'^{n-1} + E_{ijkl} \Delta\varepsilon_{kl}' \quad (4)$$

If the trial stress does not satisfy Eqn. (3), the increment of fracturing strain in direction \square can be computed using the assumption that the final stress state must satisfy Eqn. (5).

$$F_i^f = \sigma_{ii}'^n - f_{ti}' = \sigma_{ii}'^t - E_{ijkl} \Delta\varepsilon_{kl}'^f - f_{ti}' = 0 \quad (5)$$

This equation can be further simplified under the assumption that the increment of fracturing strain is normal to the failure surface, and that always only one failure surface is being checked. For failure surface \square , the fracturing strain increment has the following form.

$$\Delta \varepsilon_{ij}^{\prime f} = \Delta \lambda \frac{\partial F_k^f}{\partial \sigma_{ij}} = \Delta \lambda \delta_{ik} \quad (6)$$

After substitution into Eqn. (5) a formula for the increment of the fracturing multiplier λ is recovered.

$$\Delta \lambda = \frac{\sigma_{kk}^{\prime t} - f_{tk}^{\prime}}{E_{kkkk}} = \frac{\sigma_{kk}^{\prime t} - f_t^{\prime}(w_k^{\max})}{E_{kkkk}} \quad \text{and} \quad w_k^{\max} = L_t (\hat{\varepsilon}_{kk}^{\prime f} + \Delta \lambda) \quad (7)$$

This equation must be solved iteratively since for softening materials the value of current tensile strength $f_t^{\prime}(w_k^{\max})$ is a function of the crack opening w , and is based on Hordijk's formula [16].

The crack opening w is computed from the total value of fracturing strain $\hat{\varepsilon}_{kk}^{\prime f}$ in direction k , plus the current increment of fracturing strain $\Delta \lambda$, and this sum is multiplied by the characteristic length L_t . The characteristic length as a crack band size was introduced by Bažant and Oh [9]. Various methods were proposed for the crack band size calculation in the framework of finite element method. Feenstra [4] suggested a method based on integration point volume, which is not well suited for distorted elements. A consistent and rather complex approach was proposed by Olivier [17]. In the presented work the crack band size is calculated as a width or size of the element projected into the direction k (see Fig. 1). Červenka V. et al. [18] showed that this approach is satisfactory for low order linear elements, which are used throughout this study. They also proposed a modification, which accounts for cracks that are not aligned with element edges.

The equation (7) can be solved by recursive substitutions. It is possible to show by expanding $f_t^{\prime}(w_k^{\max})$ into a Taylor series that this iteration scheme converges as long as:

$$\left| \frac{\partial f'_t(w_k^{\max})}{\partial w} \right| < \frac{E_{kkkk}}{L_t} \quad (8)$$

Equation (8) is violated for softening materials only when snap back is observed in the stress-strain relationship, which can occur if large finite elements are used. In the standard displacement based finite element method, the strain increment is given, therefore, a snap back on the constitutive level cannot be captured. This means that the critical region, with snap back on the softening curve, will be skipped in a real calculation, which physically means, that the energy dissipated by the system will be over estimated. This is of course undesirable, and finite elements smaller than $L < E_{kkkk} / \left| \frac{\partial f'_t(0)}{\partial w} \right|$ should be used, where $\frac{\partial f'_t(0)}{\partial w}$ denotes the initial slope of the crack softening curve.

It is important to distinguish between total fracturing strain $\hat{\epsilon}'_{ij}$, which corresponds to the maximal fracturing strain reached during the loading process, and current fracturing strain ϵ'_{ij} , which can be smaller due to crack closure, and is computed using the Eqn. (9) derived by Rots and Blaauwendraad [11].

$$\epsilon'_{kl} = (E_{ijkl} + E'_{ijkl})^{-1} E_{klmn} \epsilon'_{mn}, \text{ and } E'_{ijkl} \text{ is defined by } \sigma'_{ij} = E'_{ijkl} \epsilon'_{kl} \quad (9)$$

The fourth order crack tensor E'_{ijkl} represents the cracking stiffness in the local material directions. In the current formulation, it is assumed, that there is no interaction between normal and shear components. Thus, the crack tensor is given by the following formulas.

$$E'_{ijkl} = 0 \text{ for } i \neq k \text{ and } j \neq l \quad (10)$$

Mode I crack stiffness equals

$$E_{iii}^{cr} = \frac{f_t'(w_i^{\max})}{\hat{\varepsilon}_{ii}^{f'}} \quad (11)$$

and mode II and III crack stiffness is assumed as:

$$E_{ijij}^{cr} = \frac{r_g^{ij} G}{1 - r_g^{ij}} \quad (12)$$

where $i \neq j$, $r_g^{ij} = \min(r_g^i, r_g^j)$ is minimum of shear retention factors on cracks in directions i, j , and G is the elastic shear modulus. Shear retention factor on a crack in direction i is evaluated based on the Kolmar's formula [19]:

$$r_g^i = \frac{-\ln\left(\frac{\varepsilon_{ii}'}{c_1}\right)}{c_2} \quad (13)$$

where $c_1 = 7 + 333(p - 0.005)$, $c_2 = 10 - 167(p - 0.005)$ and p is the reinforcement ratio in the interval $0 \leq p \leq 0.02$. In formulas (11) and (12), it is necessary to handle the special cases before the onset of cracking, when the expressions approach infinity. Large penalty numbers are used for crack stiffness in these cases.

The secant constitutive matrix in the material direction was formulated by Rots and Blaauwendraad [11] in the matrix format.

$$\mathbf{E}'^s = \mathbf{E} - \mathbf{E}(\mathbf{E}'^{cr} + \mathbf{E})^{-1} \mathbf{E} \quad (14)$$

Strain vector transformation matrix \mathbf{T}^ε (i.e. global to local strain transformation matrix) can be used to transform the local secant stiffness matrix to the global coordinate system.

$$\mathbf{E}^s = \mathbf{T}^{\varepsilon^T} \mathbf{E}^{s'} \mathbf{T}^{\varepsilon} \quad (15)$$

Algorithm 1: (Input is σ_{ij}^{n-1} , ε_{ij}^{n-1} , $\varepsilon_{ij}^{f^{n-1}}$, $\hat{\varepsilon}_{ii}^{f^{n-1}}$, $\Delta\varepsilon_{ij}^n$)

Find principal/material directions

if rotated model

calculate principal values and directions for $\varepsilon_{ij}^{n-1} \rightarrow \varepsilon'_{ij}$, V_{ij}

assemble coordinate transformation matrix $T_{ij} = V_{ji}$

else fixed model

recover stored coordinate transformation matrix T_{ij}

end if

Conversion to principal/material directions

$$\sigma'_{ij} = T_{ik} T_{jl} \sigma_{kl}^{n-1}, \quad \Delta\varepsilon'_{ij} = T_{ik} T_{jl} \Delta\varepsilon_{kl}^n$$

Check and calculate cracking moduli:

$$\text{for } \sigma'_{ii} > 0 \Rightarrow E'_{iii} = \frac{f'_t(w_i^{\max})}{\hat{\varepsilon}'_{ii}} \text{ and } E'_{ijj} = \frac{r_g^{ij} G}{1 - r_g^{ij}}$$

for $E'_{iii} = E'_{ijj} = \psi$, where ψ is a high penalty number

Start loop over material/principal directions $i = 1$ to 3

Store fracturing strain increment $\Delta\varepsilon_{ij}^{f \text{ stored}} = \Delta\varepsilon_{ij}^{f'}$

Assemble secant stiffness matrix and update fracturing strain increment using :

$$\mathbf{E}^{s'} = \mathbf{E} - \mathbf{E}(\mathbf{E}^{cr} + \mathbf{E})^{-1} \mathbf{E}$$

$$\Delta\varepsilon_{ij}^{f'} = \Delta\varepsilon_{ij}^{f'} + (\mathbf{E}_{ijkl} + \mathbf{E}_{ijkl}^{cr})^{-1} E_{klmn} \Delta\varepsilon'_{mn}$$

For rotated crack model correct shear terms to preserve the coaxiality of stress and strain tensors based on the formula by Willam et. al. [20]:

$$E'_{ijj} = \frac{\sigma'_{ii} - \sigma'_{jj}}{2(\varepsilon'_{ii} - \varepsilon'_{jj})}$$

Calculate trial stress state

$$\sigma''_{ij} = \sigma'_{ij} + E'_{ijkl} \Delta\varepsilon'_{kl}$$

Check Rankine criterion $\sigma''_{ii} \leq f'_t(w_i^{\max})$

If not satisfied

Find stress at the onset of cracking:

$$\beta = \frac{f'_t(w_i^{\max}) - \sigma'_{ii}}{\sigma''_{ii} - \sigma'_{ii}}, \quad \varepsilon'_{ij} = \varepsilon'_{ij} + \beta \Delta \varepsilon'_{ij}, \quad \Delta \varepsilon'_{ij} = (1 - \beta) \Delta \varepsilon'_{ij}$$

$$\sigma'_{ij} = \sigma'_{ij} + \beta(\sigma''_{ij} - \sigma'_{ij})$$

Update fracturing strain tensor based on Blaauwendraad [11]:

$$\Delta \varepsilon'^{f}_{ij} = \Delta \varepsilon'^{f}_{ij}{}^{stored} + (E_{ijkl} + E'^{tcr}_{ijkl})^{-1} E_{klmn} \Delta \varepsilon'_{mn}$$

By recursive iterations solve the following two of equations:

$$\Delta \lambda = \frac{\sigma''_{ii} - f'_t(w_i^{\max})}{E_{iiii}} \quad \text{and} \quad w_i^{\max} = L_t(\hat{\varepsilon}'^f_{ii}{}^{n-1} + \Delta \lambda)$$

Update maximal fracturing strain $\Delta \hat{\varepsilon}'_{ii} = \Delta \lambda$

Modify secant cracking moduli $E'^{tcr}_{iiii} = \frac{f'_t(w_i^{\max}) - \sigma'_{ii}}{\Delta \lambda}$

End of loop over material/principal directions

Update stress, strain and state variables

$$\sigma^n = T_{ki} T_{lj} \sigma'_{kl}, \quad \varepsilon^n_{ij} = \varepsilon^{n-1}_{ij} + \Delta \varepsilon^n_{ij}, \quad \varepsilon^{f n}_{ij} = \varepsilon^{f n-1}_{ij} + T_{ki} T_{lj} \Delta \varepsilon'_{kl}, \quad \hat{\varepsilon}'^f_{ii}{}^n = \hat{\varepsilon}'^f_{ii}{}^{n-1} + \Delta \hat{\varepsilon}'^f_{ii}$$

2.2 Plasticity model for concrete crushing

New stress state in the plastic model is computed using the predictor-corrector formula.

$$\sigma^n_{ij} = \sigma^{n-1}_{ij} + E_{ijkl}(\Delta \varepsilon_{kl} - \Delta \varepsilon^p_{kl}) = \sigma^t_{ij} - E_{ijkl} \Delta \varepsilon^p_{kl} = \sigma^t_{ij} - \sigma^p_{ij} \quad (16)$$

The plastic corrector σ^p_{ij} is computed directly from the yield function by return mapping algorithm.

$$F^p(\sigma^t_{ij} - \sigma^p_{ij}) = F^p(\sigma^t_{ij} - \Delta \lambda l_{ij}) = 0 \quad (17)$$

The crucial aspect is the definition of the return direction l_{ij} , which can be defined as

$$l_{ij} = E_{ijkl} \frac{\partial G^p(\sigma^t_{kl})}{\partial \sigma_{kl}} \quad \text{then} \quad \Delta \varepsilon^p_{ij} = \Delta \lambda \frac{\partial G^p(\sigma^t_{ij})}{\partial \sigma_{ij}} \quad (18)$$

where $G(\sigma_{ij})$ is the plastic potential function, whose derivative is evaluated at the predictor stress state σ_{ij}^t to determine the return direction.

Two failure surfaces are implemented in the current version of the material model: Drucker-Prager [21] and Menétrey-Willam [1] surface. Drucker-Prager failure criterion is defined by the function:

$$F_{DP}^p(\sigma_{ij}) = \alpha I_1 + \sqrt{J_2} - k = 0 \quad (19)$$

where I_1 and J_2 denote first invariant of the stress tensor and second deviatoric invariant respectively. The symbols α and k are parameters of the Drucker-Prager surface. The second surface is the three-parameter function of Menétrey and Willam [1].

$$F_{3P}^p = \left[\sqrt{1.5} \frac{\rho}{f_c'} \right]^2 + m \left[\frac{\rho}{\sqrt{6} f_c'} r(\theta, e) + \frac{\xi}{\sqrt{3} f_c'} \right] - c = 0 \quad (20)$$

where

$$m = \sqrt{3} \frac{f_c'^2 - f_t'^2}{f_c' f_t'} \frac{e}{e+1}, \quad r(\theta, e) = \frac{4(1-e^2) \cos^2 \theta + (2e-1)^2}{2(1-e^2) \cos \theta + (2e-1) [4(1-e^2) \cos^2 \theta + 5e^2 - 4e]^{\frac{1}{2}}}$$

In the above equations (ξ, ρ, θ) are Heigh-Vestergaard coordinates, f_c' and f_t' is compressive strength and tensile strength respectively. Parameter $e \in \langle 0.5, 1.0 \rangle$ defines the roundness of the failure surface. The failure surface has sharp corners if $e = 0.5$, and is fully circular around the hydrostatic axis if $e = 1.0$.

The position of failure surfaces is not fixed but it can move depending on the value of strain hardening/softening parameter. The strain hardening is based on the equivalent plastic strain, which is calculated according to the following formula.

$$\Delta \varepsilon_{eq}^p = \min(\Delta \varepsilon_{ij}^p) \quad (21)$$

Hardening/softening in the Drucker-Prager model is controlled by the parameter k . This parameter is selected such that the surface at the peak passes through the uniaxial compressive strength, and it changes according to the following expression.

$$k = k^0 \frac{f'_c(\varepsilon_{eq}^p)}{f'_c} \quad (22)$$

For Menétrey-Willam surface the hardening/softening is controlled by the parameter $c \in \langle 0,1 \rangle$, which evolves during the yielding/crushing process by the following relationship:

$$c = \left(\frac{f'_c(\varepsilon_{eq}^p)}{f'_c} \right)^2 \quad (23)$$

In the above two formulas the expression $f'_c(\varepsilon_{eq}^p)$ indicates the hardening/softening law, which is based on the uniaxial compressive test. The law is shown in Fig. 2. It has an elliptical ascending branch and linear descending branch after the peak. The law on the ascending branch is based on strains, while the descending branch is based on displacements to introduce mesh objectivity into the finite element solution, and its shape is based on the work of van Mier [22]. On the descending curve the equivalent plastic strain is transformed into displacements through the length scale parameter L_c . This parameter is defined analogically to the crack band parameter in the fracture model (Fig. 1), and it corresponds to the projection of element size into the direction of

minimal principal stresses. The square in the above Equation (23) is due to the quadratic nature of the Menétry-Willam surface.

Return direction is given by the following plastic potential

$$G^p(\sigma_{ij}) = \beta \frac{1}{\sqrt{3}} I_1 + \sqrt{2J_2} \quad (24)$$

where β determines the return direction. If $\beta < 0$ material is being compacted during crushing, if $\beta = 0$ material volume is preserved, and if $\beta > 0$ material is dilating. In general the plastic model is non-associated, since the plastic flow is not perpendicular to the failure surface. Only in the special case of Drucker-Prager failure function and $\beta = \alpha\sqrt{6}$, the model is associated in the sense that plastic flow is perpendicular to the Drucker-Prager failure surface.

The return mapping algorithm for the plastic model is based on predictor-corrector approach as is shown in Fig. 3. During the corrector phase of the algorithm the failure surface moves along the hydrostatic axis to simulate hardening and softening. The final failure surface has the apex located at the origin of the Haigh-Vestergaard coordinate system. Secant method based Algorithm 2 is used to determine the stress on the surface, which satisfies the yield condition and also the hardening/softening law.

Algorithm 2: (Input is $\sigma_{ij}^{n-1}, \varepsilon_{ij}^{p^{n-1}}, \Delta\varepsilon_{ij}^n$)

$$\text{Elastic predictor: } \sigma_{ij}^t = \sigma_{ij}^{n-1} + E_{ijkl} \Delta\varepsilon_{kl}^n \quad (25)$$

$$\text{Evaluate failure criterion: } f_A^p = F^p(\sigma_{ij}^t, \varepsilon_{ij}^{p^{n-1}}), \quad \Delta\lambda_A = 0 \quad (26)$$

If failure criterion is violated i.e. $f_A^p > 0$

Evaluate return direction:
$$m_{ij} = \frac{\partial G^p(\sigma_{ij}^t)}{\partial \sigma_{ij}} \quad (27)$$

Return mapping:
$$F^p(\sigma_{ij}^t - \Delta\lambda_B E m_{ij}, \varepsilon_{ij}^{p^{n-1}}) = 0 \Rightarrow \Delta\lambda_B \quad (28)$$

Evaluate failure criterion:
$$f_B^p = F^p(\sigma_{ij}^t - \Delta\lambda_B E m_{ij}, \varepsilon_{ij}^{p^{n-1}} + \Delta\lambda_B m_{ij}) \quad (29)$$

Secant iterations (i) as long as $|\Delta\lambda_A - \Delta\lambda_B| < e \quad (30)$

New plastic multiplier increment:
$$\Delta\lambda = \Delta\lambda_A - f_A^p \frac{\Delta\lambda_B - \Delta\lambda_A}{f_B^p - f_A^p} \quad (31)$$

New return direction:
$$m_{ij}^{(i)} = \frac{\partial G^p(\sigma_{ij}^t - \Delta\lambda E m_{ij}^{(i-1)})}{\partial \sigma_{ij}} \quad (32)$$

Evaluate failure criterion:
$$f^p = F^p(\sigma_{ij}^t - \Delta\lambda E m_{ij}^{(i)}, \varepsilon_{ij}^p + \Delta\lambda m_{ij}^{(i)}) \quad (33)$$

New initial values for secant iterations:

$$f_B^p < 0 \Rightarrow f_B^p = f^p, \quad \Delta\lambda_B = \Delta\lambda \quad (34)$$

$$f_B^p \geq 0 \Rightarrow f_A^p = f_B^p, \quad \Delta\lambda_A = \Delta\lambda_B, \quad f_B^p = f^p, \quad \Delta\lambda_B = \Delta\lambda \quad (35)$$

End of secant iteration loop

End of algorithm update stress and plastic strains.

$$\varepsilon_{ij}^{p^n} = \varepsilon_{ij}^{p^{n-1}} + \Delta\lambda_B m_{ij}^{(i)}, \quad \sigma_{ij}^n = \sigma_{ij}^t - \Delta\lambda_B E m_{ij}^{(i)} \quad (36)$$

2.3 Combination of plasticity and fracture model.

The objective is to combine the above models into a single model such that plasticity is used for concrete crushing and the Rankine fracture model for cracking. This problem can be generally stated as a simultaneous solution of the two following inequalities.

$$F^p(\sigma_{ij}^{n-1} + E_{ijkl}(\Delta\varepsilon_{kl} - \Delta\varepsilon_{kl}^f - \Delta\varepsilon_{kl}^p)) \leq 0 \quad \text{solve for } \Delta\varepsilon_{kl}^p \quad (37)$$

$$F^f(\sigma_{ij}^{n-1} + E_{ijkl}(\Delta\varepsilon_{kl} - \Delta\varepsilon_{kl}^p - \Delta\varepsilon_{kl}^f)) \leq 0 \quad \text{solve for } \Delta\varepsilon_{kl}^f \quad (38)$$

Each inequality depends on the output from the other one, therefore the following iterative scheme is developed.

Algorithm 3:

$$\text{Step 1: } F^p(\sigma_{ij}^{n-1} + E_{ijkl}(\Delta\varepsilon_{kl} - \Delta\varepsilon_{kl}^{f(i-1)} + b\Delta\varepsilon_{kl}^{cor(i-1)} - \Delta\varepsilon_{kl}^{p(i)})) \leq 0 \quad \text{solve for } \Delta\varepsilon_{kl}^{p(i)}$$

$$\text{Step 2: } F^f(\sigma_{ij}^{n-1} + E_{ijkl}(\Delta\varepsilon_{kl} - \Delta\varepsilon_{kl}^{p(i)} - \Delta\varepsilon_{kl}^{f(i)})) \leq 0 \quad \text{solve for } \Delta\varepsilon_{kl}^{f(i)}$$

$$\text{Step 3: } \Delta\varepsilon_{ij}^{cor(i)} = \Delta\varepsilon_{ij}^{f(i)} - \Delta\varepsilon_{ij}^{f(i-1)} \quad (39)$$

Iterative correction of the strain norm between two subsequent iterations can be expressed as

$$\left(\Delta\varepsilon_{ij}^{cor(i)}\right) = (1-b)\alpha^f\alpha^p\left(\Delta\varepsilon_{ij}^{cor(i-1)}\right) \quad (40)$$

$$\text{where } \alpha^f = \frac{\left\|\Delta\varepsilon_{ij}^{f(i)} - \Delta\varepsilon_{ij}^{f(i-1)}\right\|}{\left\|\Delta\varepsilon_{ij}^{p(i)} - \Delta\varepsilon_{ij}^{p(i-1)}\right\|}, \quad \alpha^p = \frac{\left\|\Delta\varepsilon_{ij}^{p(i)} - \Delta\varepsilon_{ij}^{p(i-1)}\right\|}{\left\|\Delta\varepsilon_{ij}^{cor}\right\|}$$

and b is an iteration correction or relaxation factor, which is introduced in order to guarantee convergence. It is to be determined based on the run-time analysis of α^f and

α^p , such that the convergence of the iterative scheme can be assured. The parameters α^f and α^p characterize the mapping properties of each model (i.e. plastic and fracture). It is possible to consider each model as an operator, which maps strain increment on the input into a fracture or plastic strain increment on the output. The product of the two mappings must be contractive in order to obtain a convergence. The necessary condition for the convergence is:

$$\left((1-b)\alpha^f\alpha^p \right) < 1 \quad (41)$$

If b equals 0, an iterative algorithm based on recursive substitution is obtained. The convergence can be guaranteed only in two cases:

- (1) One of the models is not activated (i.e. implies α^f or $\alpha^p = 0$),
- (2) There is no softening in either of the two models and dilating material is not used in the plastic part, which for the plastic potential in this work means $\beta \leq 0$ (see Eqn. (24)). This is a sufficient but not necessary condition to ensure that α^f and $\alpha^p < 1$.

It can be shown that the values of α^f and α^p are directly proportional to the softening rate in each model. Since the softening model remains usually constant for a material model and finite element, their values do not change significantly between iterations. It is possible to select the scalar b such that the inequality (41) is satisfied always at the end of each iteration based on the current values of α^f and α^p . There are three possible scenarios, which must be handled, for the appropriate calculation of b :

- (1) $\left| \alpha^f\alpha^p \right| \leq \chi$, where χ is related to the requested convergence rate. For linear rate it can be set to $\chi = 1/2$. In this case the convergence is satisfactory and $b = 0$.

(2) $\chi < |\alpha^f \alpha^p| < 1$, then the convergence would be too slow. In this case b can

be estimated as $b = 1 - \frac{|\alpha^f \alpha^p|}{\chi}$, in order to increase the convergence rate.

(3) $1 \leq |\alpha^f \alpha^p|$, then the algorithm is diverging. In this case b should be calculated

as $b = 1 - \frac{\chi}{|\alpha^f \alpha^p|}$ to stabilize the iterations.

This approach guarantees convergence as long as the parameters α^p, α^f does not change drastically between the iterations, which should be satisfied for smooth and correctly formulated models. The rate of convergence depends on material brittleness, dilating parameter β and finite element size. It is advantageous to further stabilize the algorithm by smoothing the parameter b during the iterative process:

$$b = (b^{(i)} + b^{(i-1)})/2 \quad (42)$$

where the superscript i denotes values from two subsequent iterations. This will eliminate problems due to the oscillation of the correction parameter b . Important condition for the convergence of the above Algorithm 3 is that the failure surfaces of the two models are intersecting each other in all possible positions even during the hardening or softening.

Additional constraints are used in the iterative algorithm. If the stress state at the end of the first step violates the Rankine criterion, the order of the first two steps in 3 is reversed. Also in reality concrete crushing in one direction has an effect on the cracking in other directions. It is assumed that after the plasticity yield criterion is violated, the tensile strength in all material directions is set to zero.

On the structural level secant matrix is used in order to achieve a robust convergence during the strain localization process.

The proposed algorithm for the combination of plastic and fracture models is graphically shown in Fig. 4. When both surfaces are activated, the behavior is quite similar to the multi-surface plasticity (Simo et al. [23]). Contrary to the multi-surface plasticity algorithm the proposed method is more general in the sense that it covers all loading regimes including physical changes such as for instance crack closure. Currently, it is developed only for two interacting models, and its extension to multiple models is not straightforward

3. Fracturing Rate Effect and Creep for Dynamic Loading

For fast loading rates that can occur in dynamic loading types, such as ground shocks, missile penetration etc, it is important to consider two phenomena that affects the stress-strain relations for concrete: (1) rate dependence of crack growth and (2) visco-elasticity or creep of the intact material between the cracks.

The rate effect is handled similarly to the approach proposed by Caner [26], where it was suggested to described the rate dependence as:

$$\dot{w} = k_o \sinh \left(\frac{T_0}{T} \frac{\sigma - f_t^{r0}(w)}{k_r N_b(w)} \right) e^{-\frac{Q}{R} \left(\frac{1}{T} - \frac{1}{T_0} \right)} \quad (43)$$

where $\dot{w} = dw/dt$, t = time, σ is cohesive crack stress, k_o, k_r = material constants, T is absolute temperature, T_0 is the reference temperature at which the softening law $f_t^{r0}(w)$ was determined; R is the universal gas constant; Q is the activation energy of interatomic bond ruptures, and $N_b(w)$ is the number of surviving bonds across the

cohesive crack per unit area. The equation (43) can be imagined to correspond to a rheologic model, in which a rate-independent cohesive crack element is coupled in parallel with a nonlinear dashpot at each point along the cohesive crack zone. After several mathematical manipulations in analogy to Caner [26], it is possible to arrive to the following simple scaling functions:

$$F(w) = F^0(w) \left[1 + C_2 \ln \left(\frac{2\dot{w}}{w C_1} \right) \right] \quad (44)$$

$$F = F^0 \left[1 + C_2 \ln \left(\frac{2\dot{\varepsilon}}{\varepsilon C_1} \right) \right] \quad (45)$$

The first scaling law (44) will be used to scale the softening laws of the combined model since they depend on displacements. The same scaling law will be used for tensile softening as well as the compressive softening. This seems to be an acceptable assumption since the compressive failure is also dominated by the development of tensile microcracks.

The second scaling law (45) will be used for the scaling of the failure surfaces in the fracturing as well as in the plastic model.

The following assumptions and simplifications were used to derive the above rate effect scaling laws:

The function $N_b(w)$ is approximated to be proportional to the softening law $f_t'^0(w)$ through the constant C_b .

$$N_b(w) = C_b f_t'^0(w)$$

It is assumed that the material temperature is not very different from the temperature during which the material parameters were determined, i.e. $T \approx T_0$. As a consequence to this assumption it is possible to set:

$${}^{\varepsilon}C_1 = \frac{k_0}{s_{cr}} e^{-\frac{Q}{R}\left(\frac{1}{T} - \frac{1}{T_0}\right)} \approx \frac{k_0}{s_{cr}}, \quad {}^wC_1 = k_0 e^{-\frac{Q}{R}\left(\frac{1}{T} - \frac{1}{T_0}\right)} \approx k_0$$

$$C_2 = k_r C_b \frac{T}{T_0} \approx C_r$$

The elastic strain rate is negligible comparing to the cracking strain rate:

$$\dot{\varepsilon} = \frac{\dot{w}}{s_{cr}} + \frac{\dot{\sigma}}{E} \approx \frac{\dot{w}}{d_{\max}}$$

where s_{cr} is the average micro crack spacing, which is assumed to be equal to the maximal aggregate size. This assumption is used only to scale the initial failure surfaces, therefore it seems to be acceptable, since before the peak strength is used there is no localization and the microcracking usually starts between concrete matrix and aggregates.

Finally the sinh function was eliminated by the assumption:

$$\sinh(x) = \ln(x + \sqrt{x^2 + 1}) = \ln(2x), \quad \text{for } x^2 \gg 1$$

This assumption is valid if the loading rate is much larger than the parameter C_1 .

The creep of the elastic material between the cracks is considered in analogy to the approach proposed by Caner [26] for the microplane model. The method is modified for the fracture-plastic combined model. Long time creep is of no interest for dynamic loading types, therefore, the entire Maxwell chain is not needed and a single spring-

dampner Maxwell rheological model is sufficient. For uniaxial stress state the model reads:

$$\dot{\varepsilon} = \frac{\dot{\sigma}}{E} + \frac{\sigma}{\eta} \quad (46)$$

where η represents the material viscosity.

If it is assumed that the strain rate $\dot{\varepsilon}$ remains constant during a time step, the solution of the equation (46) at time t_n can be written as:

$$\sigma(t) = \eta \dot{\varepsilon} + \left(\sigma_i - \eta \dot{\varepsilon} \right) e^{-E(t-t_n)/\eta} \quad (47)$$

Then a quasi-elastic incremental stress strain relation can be written:

$$\sigma_n = \sigma_{n-1} + E'' \Delta \varepsilon_n - \Delta \sigma'' \quad (48)$$

where:

$$E'' = \frac{1 - e^{-\Delta t/\tau_1}}{\Delta t/\tau_1} E, \quad \Delta \sigma'' = \left(1 - e^{-\Delta t/\tau_1} \right) \sigma_n, \quad \tau_1 = \frac{\eta}{E} \quad (49)$$

The formula (48) is used to calculate the trial stress state in the fracturing and plastic models:

$$\sigma_{ij}^t = \frac{E''}{E} E_{ijkl} \Delta \varepsilon_{kl}^n + e^{-\Delta t/\tau_1} \sigma_{ij}^n = \chi_0 E_{ijkl} \Delta \varepsilon_{kl}^n + \chi_1 \sigma_{ij}^n \quad (50)$$

where parameters χ_0 and χ_1 are identical to 1 if static loading is considered. The trial stress predictions in Algorithms 1 and 2 should be modified by including the new parameters χ_0 and χ_1 for consideration of short term creep effects.

4. Model Testing

A constitutive driver was developed for testing various stress-strain loading histories in order to investigate the behavior of the proposed model. In this section, the constitutive driver is used to explore the numerical behavior of the proposed algorithm for the combination of the fracture and plastic models. Three selected scenarios are considered:

- (1) Uni-axial compression with large load steps, unloading into tension and then reloading again into compression (Fig. 5). Robust material model for finite element solution must be able to handle large strain increments with physical changes, since it is generally not possible to guarantee that small strain increments will be sent to the material model. Even if very small loading steps are used on the structural level, large strain increment can occur locally due to stress redistribution. This is especially true for softening and brittle materials, where strain localization can occur quite suddenly and can have an explosive character. Fig. 5 shows also the stress-strain curve when small strain increments are used.
- (2) Crack closure due to crushing in other material direction (Fig. 7). In this example crack is introduced in one direction (x direction). After the crack is fully opened and no more stresses can be transferred across the crack, compressive strains are applied in direction y . After crushing starts the plastic strains will ultimately close the crack in direction x . The third material direction z will be kept free, which means $\sigma_{zz} = 0$ condition will be enforced. After the crack in direction x closes, a bi-axial compression state should be recovered. At this point the stress σ_{yy} should increase until it reaches a softening branch, which corresponds to the appropriate bi-axial stress state.

(3) Third example is loaded in all three material directions (Fig. 9). Equivalent magnitudes of strain increments are applied in two tensile directions x , y and compression direction z . This means that all three surfaces and both models are active. The cracks are opening in directions x and y , but at the same time they are always partially closed by plastic strains induced by the crushing in direction z .

The stress strain diagrams for the three examples are shown in Fig. 5,7 and 9. Fig. 6,8 and 10 show the evolution of stress error and the parameters α^f , α^p and b during the iterative process at the most critical points during the loading history. The examples clearly show that the combined algorithm converges very quickly. In the worst case of tri-axial loading and fully damaged material, 12 iterations are needed to satisfy the convergence criterion, which is set to 1% difference in stresses between the two models.

5. Applications

This section contains examples of two applications of the presented model to the simulation of real behavior of concrete structures. First example is a non-linear analysis of liner anchor experiment. The second example is a simulation of experimental specimen for testing pre-stressing cable anchoring. Another application of this model to the analysis of powder actuated anchors was described by Červenka et al. [24].

5.1 Containment liner anchor

In nuclear containment vessels steel liner is attached to the concrete using T-shaped line anchors. Load-carrying capacity of these anchors is usually determined by experiments (Fig. 14). Experiments are performed for a single anchor, while in reality there are

many anchors in the containment vessel, and it can be expected that an anchor behavior may be affected by neighboring anchors. The experimental setup was design using non-linear two-dimensional analyses with the program SBETA [18,25], such that the behavior of the experimentally tested single anchor is similar to the behavior of the real anchor in the containment vessel. The combined fracture-plastic concrete model, which is described in this paper, was used in three-dimensional numerical studies to verify some of the assumption in the two-dimensional analyses: namely, the increase of compressive strength and ductility due to three-dimensional confinement in front of the anchor. The specimen geometry is shown in Fig. 11. The specimen was supported along its bottom and right edges and by a spring, which was located to the left of the anchor. The purpose of this spring support was to simulate the effect of other anchors in a real containment vessel. The location and the spring stiffness value were determined by the two-dimensional analysis with SBETA program. The specimen was loaded by horizontal force at the right end of the liner up to the failure. The load-displacement diagrams are compared in Fig. 13 and they show a very good agreement of numerical and experimental results. Cracking and crushing patterns are shown in Fig. 15, and they compare well with the experimental failure pattern in Fig. 14. Cracking started at the left edge of the anchor bottom flange and it propagated towards a spring support. The final failure occurred by compressive crushing of concrete to the right of the anchor.

5.2 Pre-stressing cable anchor

The combined fracture-plastic material model was applied to the non-linear three-dimensional analysis of pre-stressing cable anchors. Pre-stressing force is transferred from pre-stressing cables to concrete through special cylindrical anchors, which are embedded into concrete during casting. Shape of the anchor is shown in Fig. 16 along

with the finite element model. The objective of the analysis was to simulate experiments, which are undertaken during the anchor validation process. In the experiment, the pre-stressing cable anchor is embedded into a concrete block. Anchor is surrounded by a reinforcement spiral, and it is loaded by compressive forces at the top to simulate the action of pre-stressing. The numerical load-displacement curve is shown in Fig. 17, where it is possible to see a very good agreement of analytical and experimental peak loads. It was not possible to compare load-displacement curves, since the experimental curve was not available to the authors. The final failure pattern was due to radial cracking and crushing shear failure around the anchor, and it is shown in Fig. 18.

5.3 Powder actuated anchors

Powder actuated anchors are inserted into the intact concrete by explosion. Behavior simulation of these anchors was an objective of a cooperative project between Cervenka Consulting and University of Stuttgart. During the insertion phase the friction between steel and concrete causes high temperatures in the steel and partial melting of the material near the outer surface of the anchor. This causes mixing of the two materials: concrete and steel. Therefore, there is no distinct boundary and a very good bond between the two materials. Thus the load carrying capacity of the anchor is mainly given by the strength of the highly damaged concrete surrounding the end of the nail. This was also the objective of the presented analysis: to simulate concrete crushing and cracking around the anchor. The material changes, which occur on the contact between steel and concrete during the fast insertion, are not addressed by this study.

Anchors are simulated by axi-symmetrical and 3D analyses. The geometry of the problem is shown in Fig. 19. The anchor is inserted into a pre-drilled hole by explosion.

This insertion phase was simulated by expanding a hole with zero initial radius by prescribing horizontal displacements at the finite element nodes at the location of the anchor head.

The second phase (i.e. anchor pull-out) was modeled by prescribing vertical displacements along the nodes, which again correspond to the anchor head.

The load-displacement for the pull-out phase are compared with the experimental results in Fig. 20. It should be noted that this excellent agreement is obtained using the standard values of material parameters $f_c' = 25.5\text{MPa}$, $f_t' = 2.32\text{MPa}$, $E = 30316\text{MPa}$, $\nu = 0.12$, $G_f = 100\text{N/m}$ and $w_d = -0.5\text{mm}$. The only parameter, for which experimental data or formulas are not available is the parameter β (see the Eqn. (24)), which defines the plastic flow. By inverse analysis an optimal value of this parameter is computed to be $\beta = 0$, which physically means that the material volume is preserved during the plastic flow.

Fig. 21 shows the evolution of circumferential stresses at various load steps and Fig. 22 show the distribution of minimal principal stresses at load step 19 (i.e. end of the expansion phase). Maximal compressive stresses in the analysis are around -350MPa .

6. Conclusions

A combined material model for concrete was presented, which includes a smeared crack model for concrete cracking and Drucker-Prager or Menétrey-Willam plasticity model for concrete crushing. Both models are formulated separately and a general algorithm is devised to iteratively determine the separation of the strain increment into the fracturing and plastic part. The behavior of this algorithm was demonstrated on several critical loading histories. The algorithm is effective and stable even when very large load steps are used or when physical changes occur during the loading. This model was successfully applied to the analysis of liner anchors in nuclear containment vessel, to the analysis of pre-stressing cable anchoring and to the analysis of powder actuated anchors, which are inserted to concrete by explosion. It was possible to simulate both qualitatively and quantitatively the behavior of this wide range of anchoring problems.

7. References

1. Menétrey, P., Willam, K.J., Triaxial failure criterion for concrete and its generalization. *ACI, Structural Journal*, 1995, **92(3)**, pp 311-318.
2. Pramono, E, Willam, K.J., Fracture Energy-Based Plasticity Formulation of Plain Concrete, *ASCE-JEM*, 1989, **115**, pp 1183-1204.
3. Menétrey, Ph., Walther, R., Zimmermann, Th., Willam, K.J., Regan, P.E. Simulation of punching failure in reinforced concrete structures. *Journal of Structural Engineering*, 1997, **123(5)**, pp 652-659.

4. Feenstra, P.H., *Computational Aspects of Bi-axial Stress in Plain and Reinforced Concrete*. PhD Thesis, Delft University of Technology, 1993.
5. Feenstra, P.H., Rots, J.G., Amesen, A., Teigen, J.G., Hoiseth, K.V., A 3D Constitutive Model for Concrete Based on Co-rotational concept. *Proc. EURO-C 1998*, **1**, pp. 13-22.
6. Etse, G., *Theoretische und numerische Untersuchung zum diffusen und lokalisierten Versagen in Beton*, PhD Thesis, University of Karlsruhe 1992.
7. Rashid, Y.R., Ultimate Strength Analysis of Prestressed Concrete Pressure Vessels, *Nuclear Engineering and Design*, 1968, **7**, pp 334-344.
8. Červenka, V., Gerstle, K., Inelastic Analysis of Reinforced Concrete Panels: Part I: Theory, *Publication I.A.B.S.E.*, 1971, 31, pp 32-45.
9. Bažant, Z.P., Oh, B.H., Crack Band Theory for Fracture of Concrete, *Materials and Structures, RILEM*, Paris, France, 1983, **16**, pp 155-177.
10. de Borst, R., *Non-linear analysis of frictional materials*, PhD Thesis, Delft University of Technology, 1986.
11. Rots, J.G. and Blaauwendraad, J., Crack models for concrete: discrete or smeared? Fixed, multi-directional or rotating? *HERON* 1989, **34(1)**.
12. Owen, J.M., Figueiras, J.A., Damjanic, F., Finite Element Analysis of Reinforced and Prestressed concrete structures including thermal loading, *Comp. Meth. Appl. Mech. Eng.*, 1983, **41**, pp 323-366.
13. Simo, J.C., Ju, J.W., Strain and Stress-based Continuum Damage Models-I. Formulation, II-Computational Aspects, *Int. J. Solids Structures*, 1987, **23(7)**, pp 821-869.

14. Meschke, G., Lackner, R., Mang, H.A., An Anisotropic Elastoplastic-Damage Model for Plain Concrete, *Int. J. Num. Meth. Eng.*, 1998, **42**, pp 703-727.
15. Wilkins, M.L., Calculation of Elastic-Plastic Flow, *Methods of Computational Physics*, **3**, Academic Press, New York, 1964.
16. Hordijk, D.A., *Local Approach to Fatigue of Concrete*, PhD Thesis, Delft University of Technology, The Netherlands, 1991.
17. Olivier, J., A Consistent Characteristic Length For Smearred Cracking Models, *Int. J. Num. Meth. Eng.*, 1989, **28**, pp 461-474.
18. Červenka, V., Pukl, R., Ozbolt, J., Eligehausen, R., Mesh Sensitivity Effects in Smearred Finite Element Analysis of Concrete Structures, Proc. FRAMCOS 2, 1995, pp 1387-1396.
19. Kolmar, W., *Beschreibung der Kraftuebertragung ueber Risse in nichtlinearen Finite-Element-Berechnungen von Stahlbetontragwerken*, PhD Thesis, T.H. Darmstadt, 1986, pp 94.
20. Willam, K, Pramono, E., and Sture, S., Fundamental issues of smearred crack models, Fracture of Concrete and Rock, Eds. S.P. Shah and S.E. Swartz, Springer-Verlag, 1989, pp. 192-207.
21. Drucker, D.C., Prager, W., Soil Mechanics and Plastic Analysis or Limit Design, *Q. Appl. Math.*, 1952, 10(2), pp 157-165.
22. van Mier J.G.M. Multi-axial Strain-softening of Concrete, Part I: fracture, *Materials and Structures, RILEM*, 1986, **19(111)**.

23. Simo, J.C., Kennedy, J.G., Govindjee, S., Non-smooth Multisurface Plasticity and Viscoplasticity. Loading/unloading Conditions and Numerical Algorithms, *Int. J. Num. Meth. Eng.*, 1988, **26**, pp 2161–2185.
24. Červenka, J, Červenka, V., Eligehausen, R., Fracture-Plastic Material Model for Concrete, Application to Analysis of Powder Actuated Anchors, Proc. FRAMCOS 3, 1998, pp 1107-1116.
25. Margoldova, J., Červenka, V., Pukl, R., Applied Brittle Analysis, *Concrete Eng. International*, November/December 1998.
26. Caner, F.,C., *Computational Modeling of Damage and Fracture in Concrete*, PhD thesis, Northwestern University, 2000.

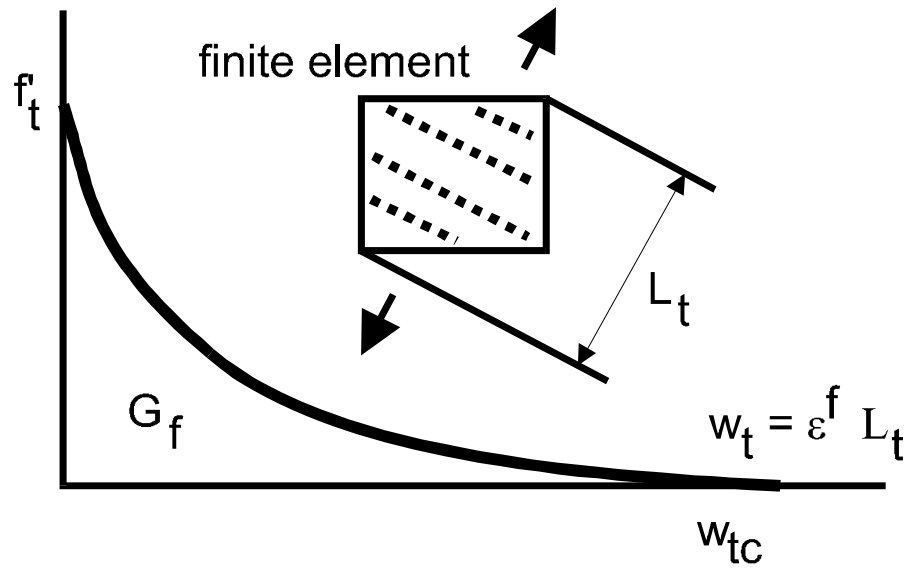


Fig. 1. Tensile softening and characteristic length

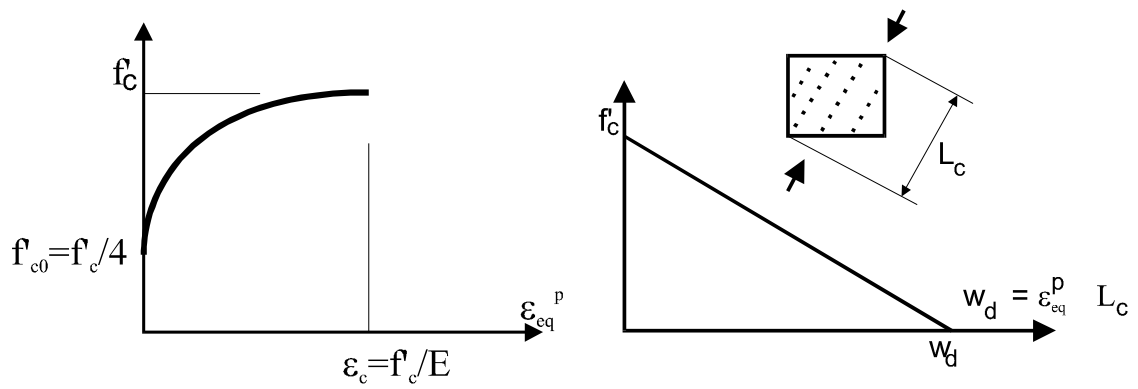


Fig. 2. Compressive hardening/softening and compressive characteristic length. Based on experimental observations by van Mier [21].

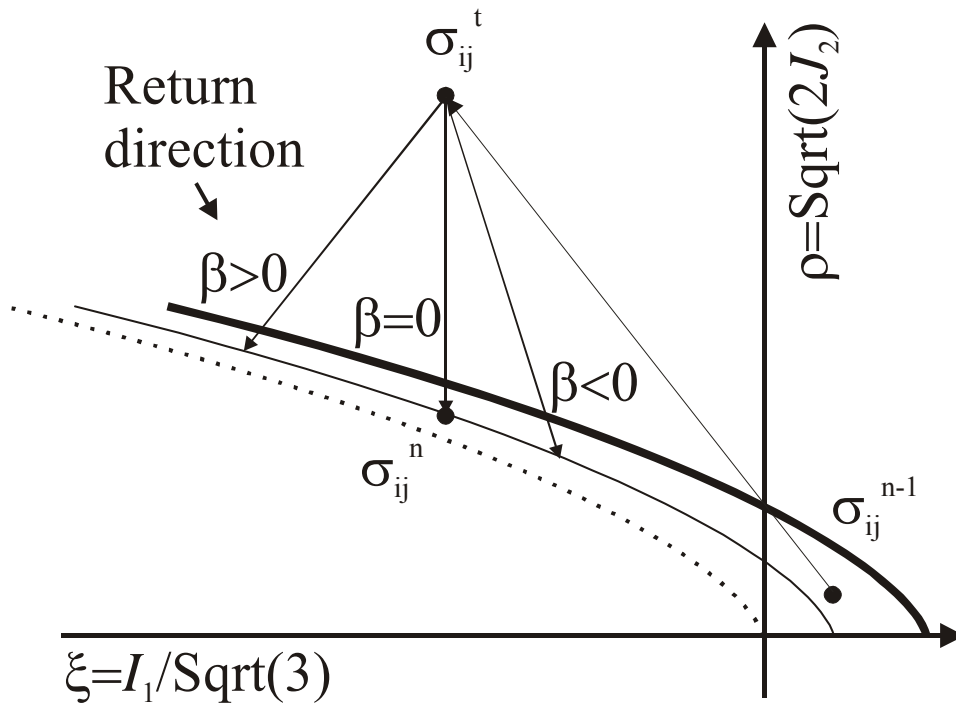


Fig. 3. Plastic predictor-corrector algorithm.

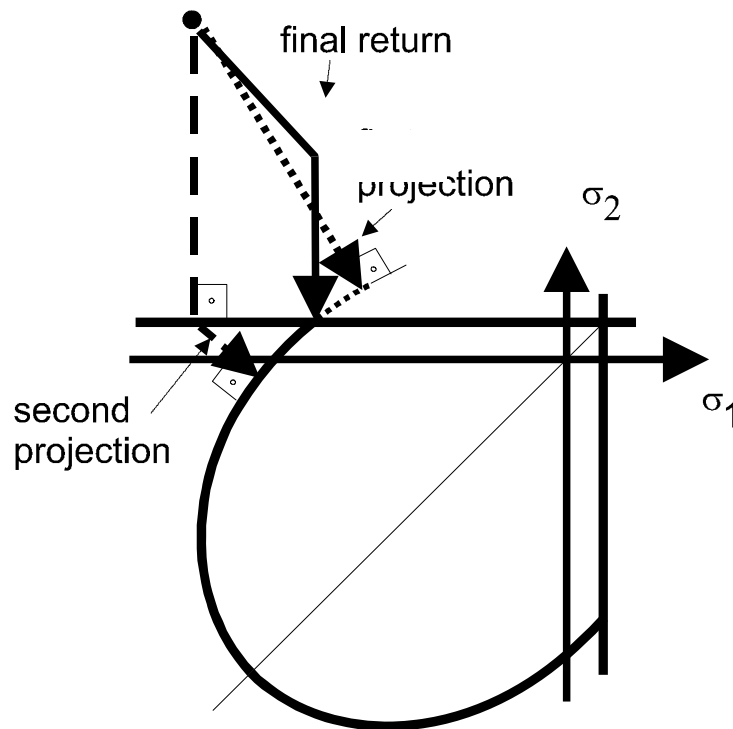


Fig. 4. Schematic description of the iterative process (39). For clarity shown in two dimensions.

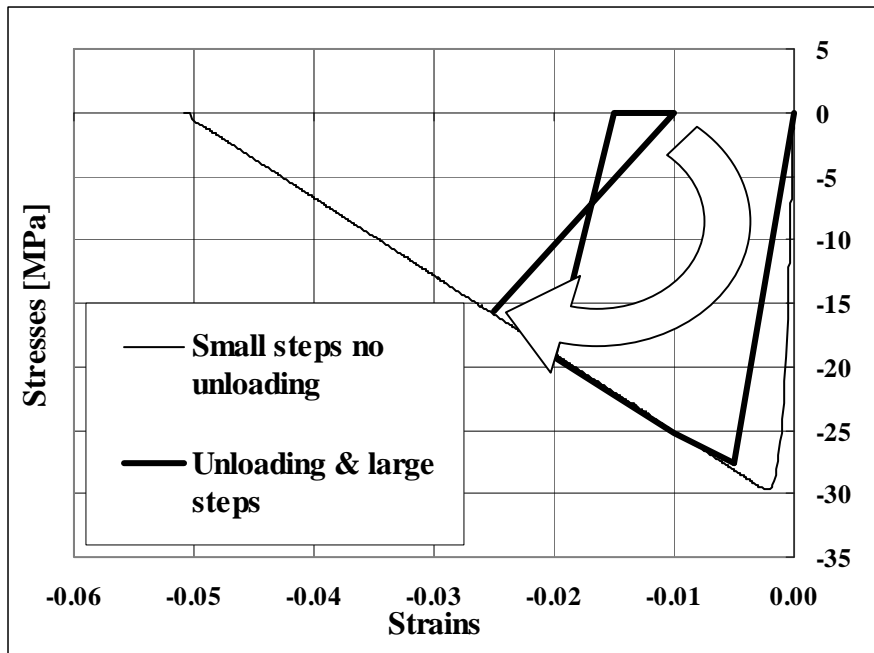


Fig. 5. Uni-axial compression example with large load steps.

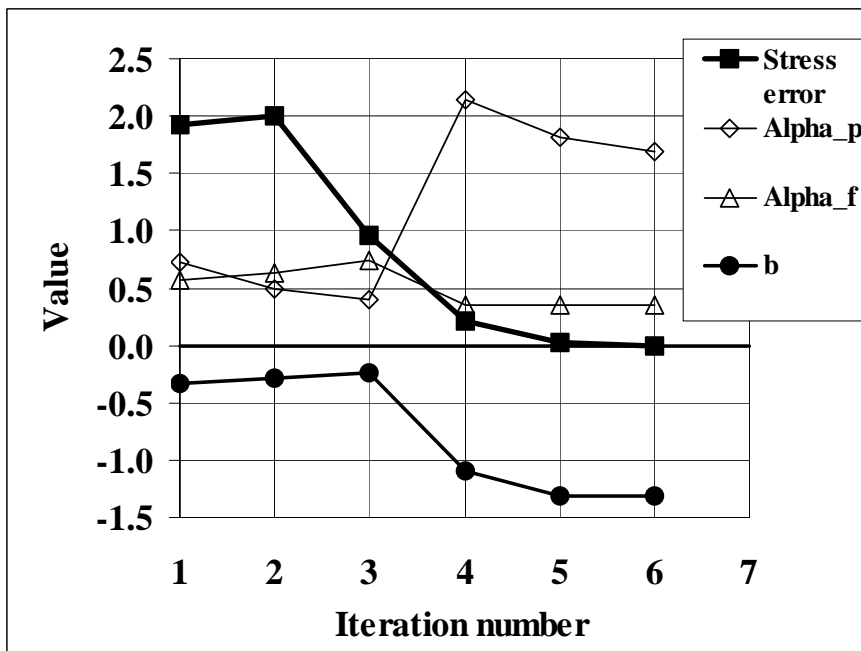


Fig. 6. Evolution of parameters α^f , α^p , and b during the large step in the uni-axial compression test (Fig. 5).

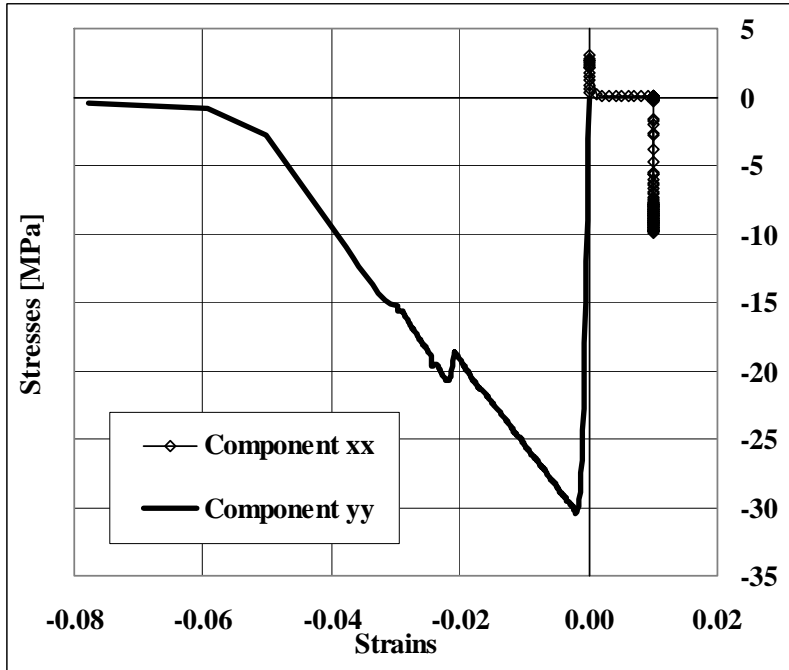


Fig. 7. Bi-axial example with crack closure due to concrete crushing.

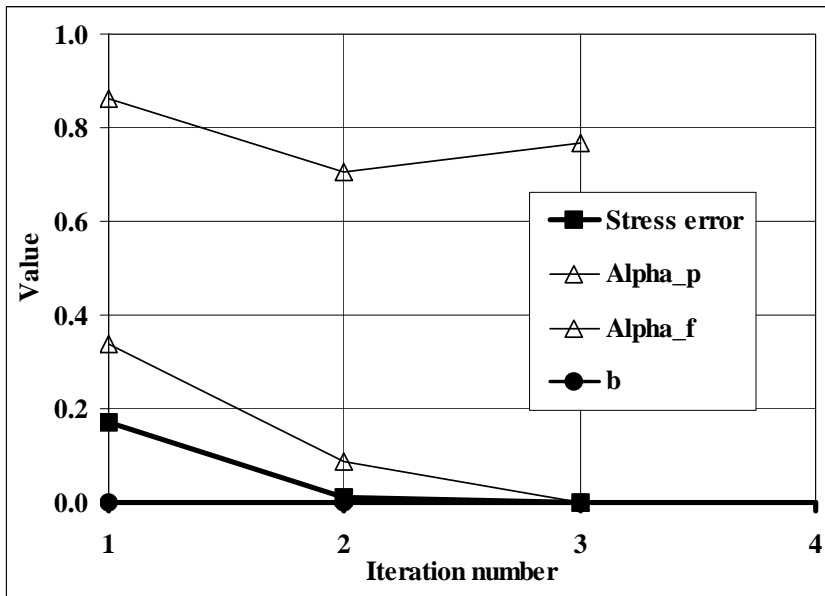


Fig. 8. Evolution of parameters parameters α^f , α^p , and b during the load step with crack closure in the bi-axial example (Fig. 7).

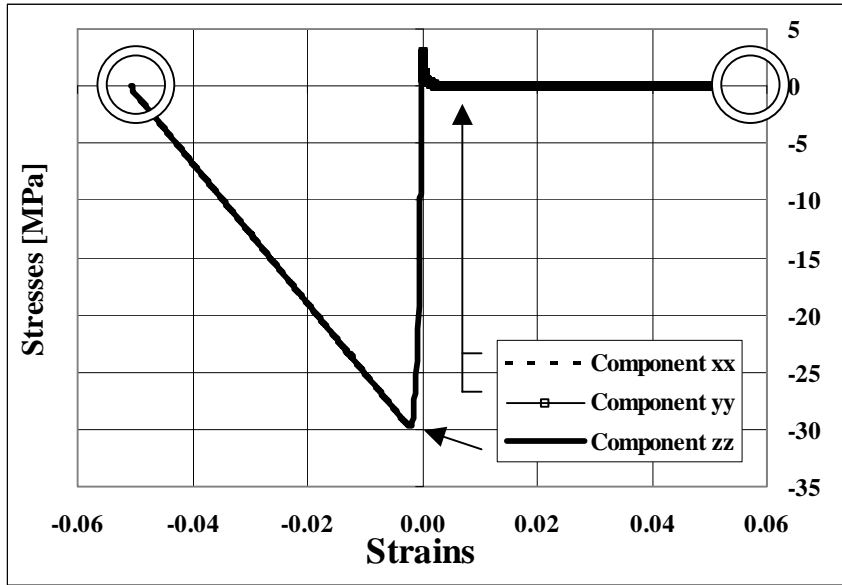


Fig. 9. Tri-axial example with complete damage of the material.

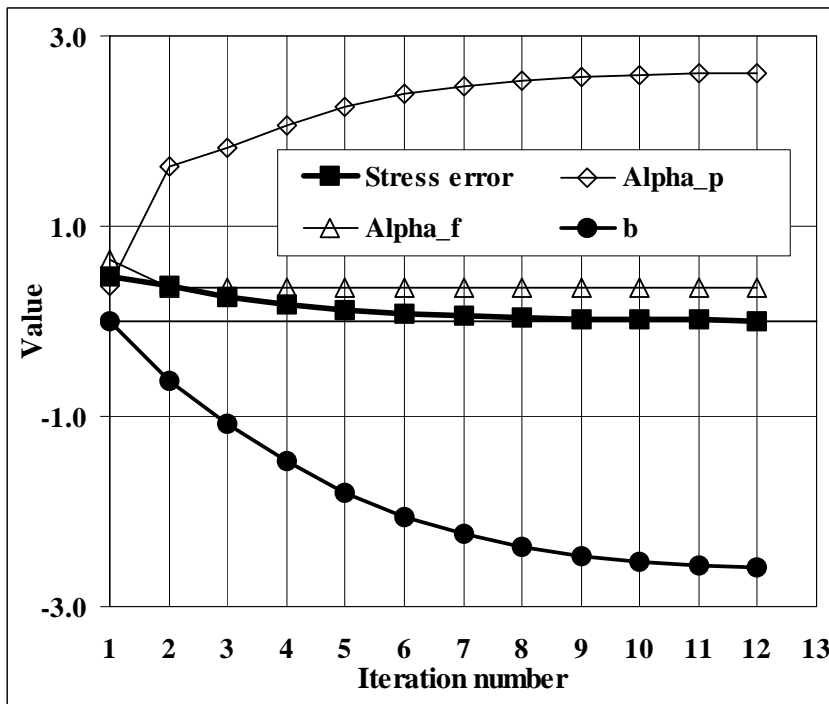


Fig. 10. Evolution of parameters parameters α^f , α^p , and b during the last load step in the tri-axial example (Fig. 9).

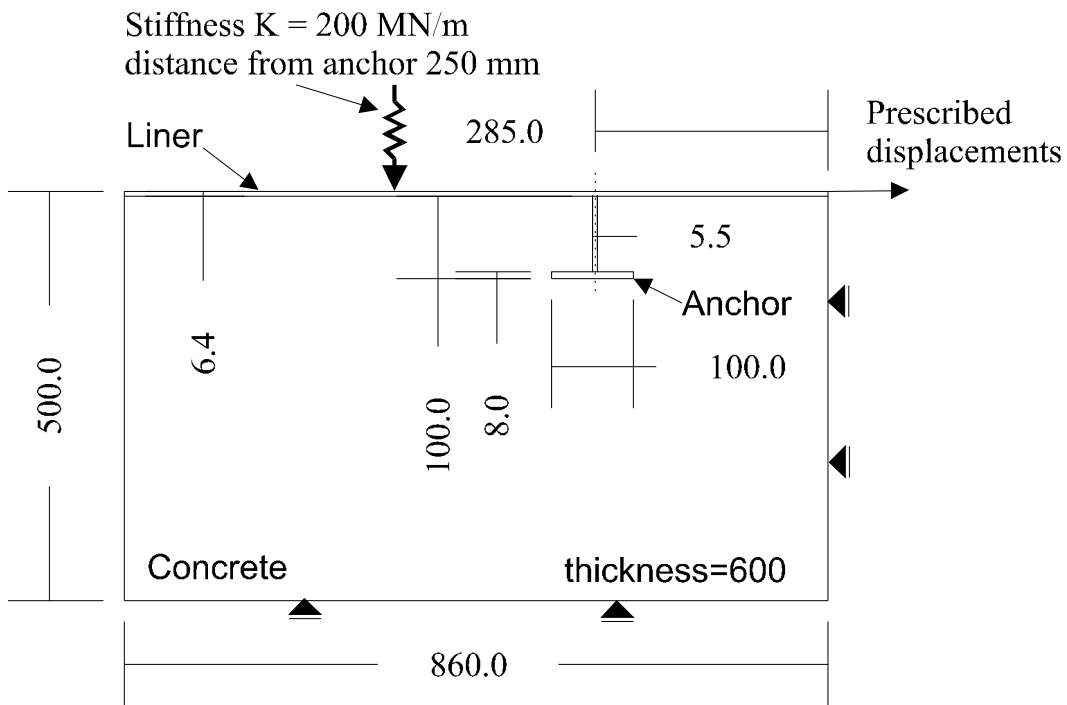


Fig. 11. Geometry of the liner anchor experiment. Dimensions in mm.

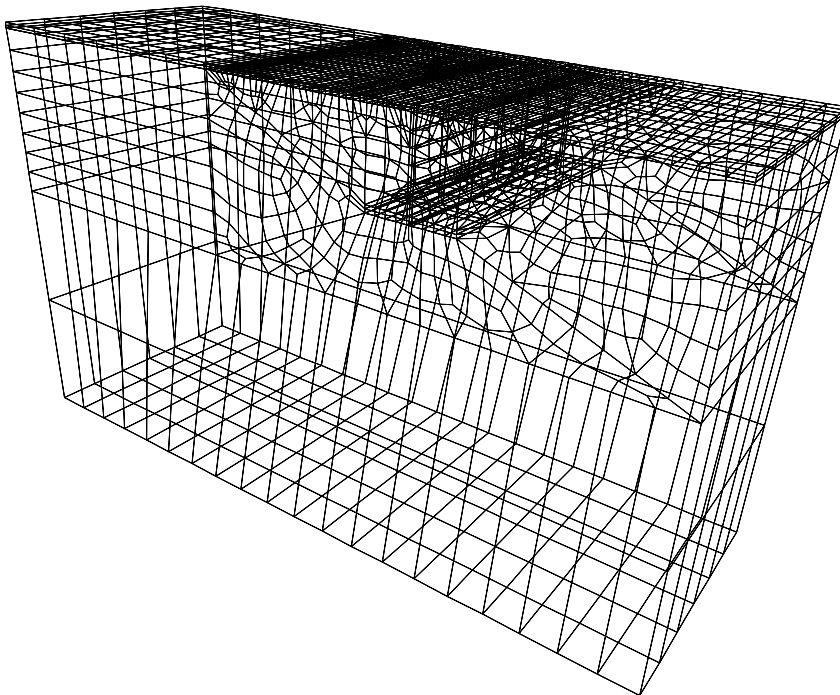


Fig. 12. Three-dimensional finite element model, which was used for the liner anchor analysis.

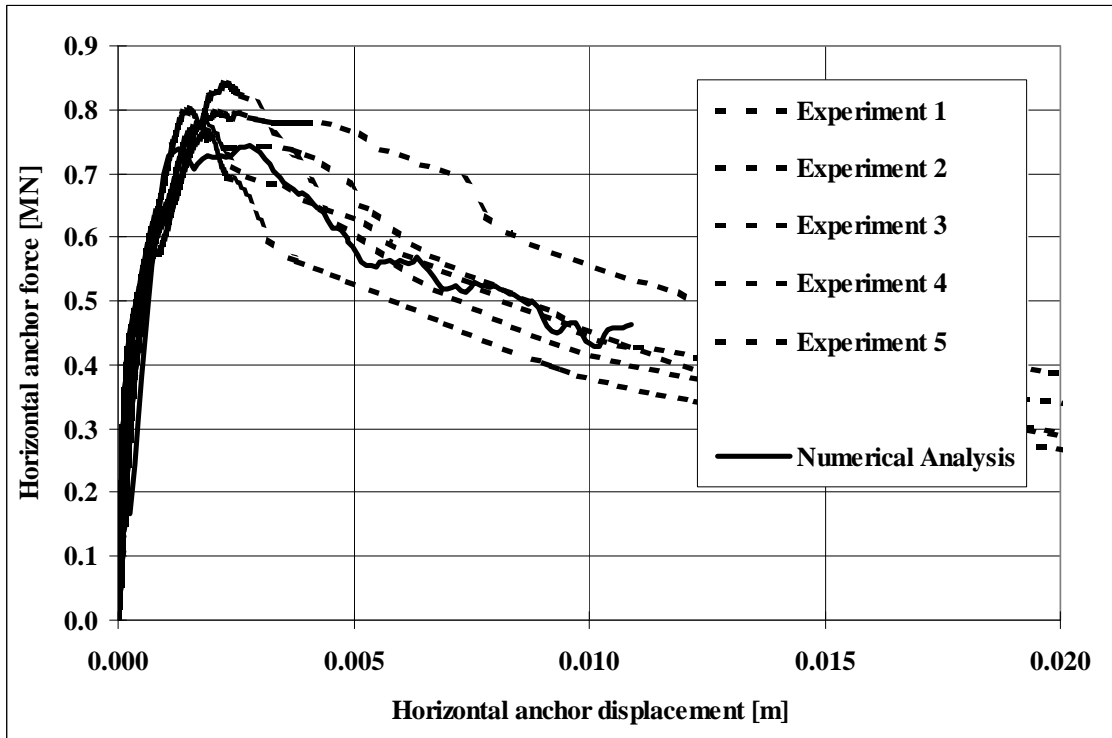


Fig. 13. Load-displacement diagram for liner anchor three-dimensional analysis and comparison with experimental data. (Experimental data are courtesy of Ishikawajima Harima Heavy Industries and Tokyo Electric Power Company).

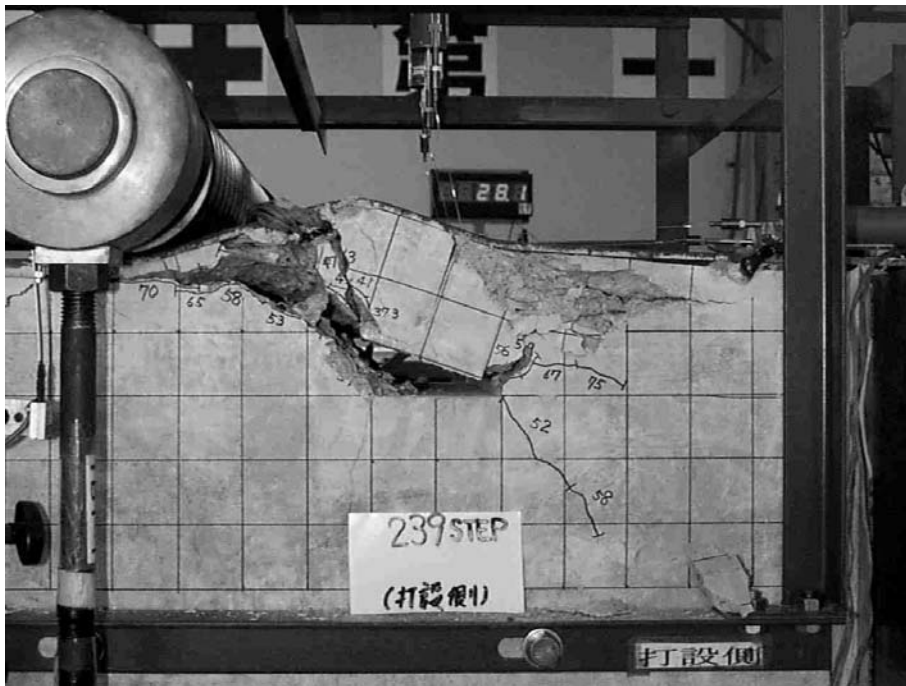


Fig. 14. Failure pattern in liner anchor experiments. (Photo: courtesy of Ishikawajima Harima Heavy Industries and Tokyo Electric Power Company)

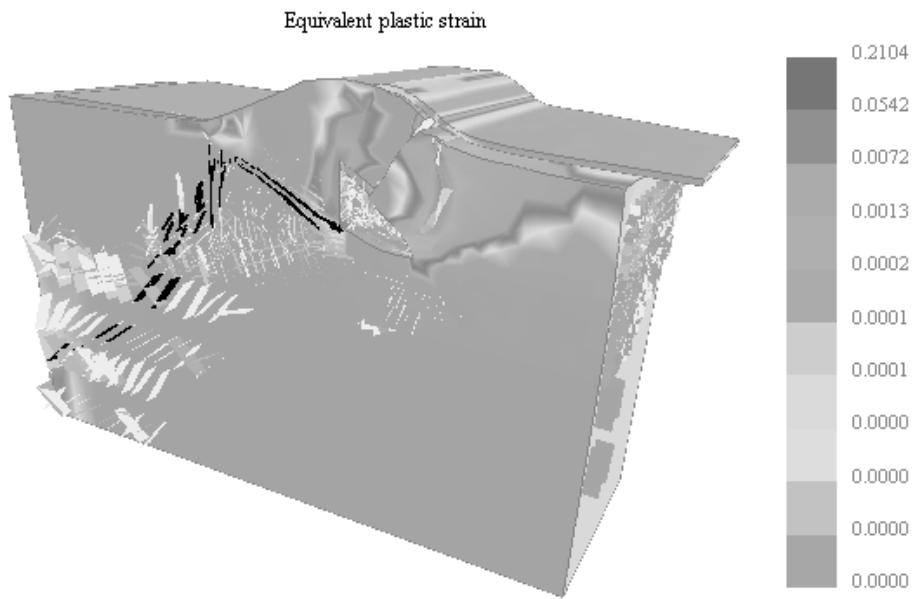


Fig. 15. Failure mode for liner anchor analysis. Shows concrete cracking and crushing at the end of the analysis.

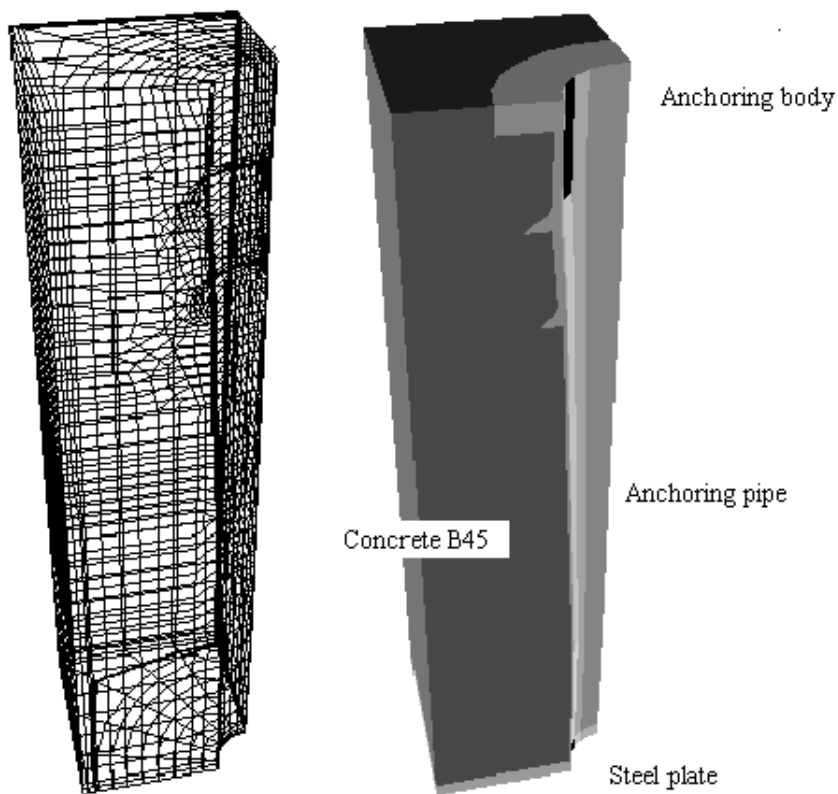


Fig. 16. Finite element model for the pre-stressing cable anchor analysis.

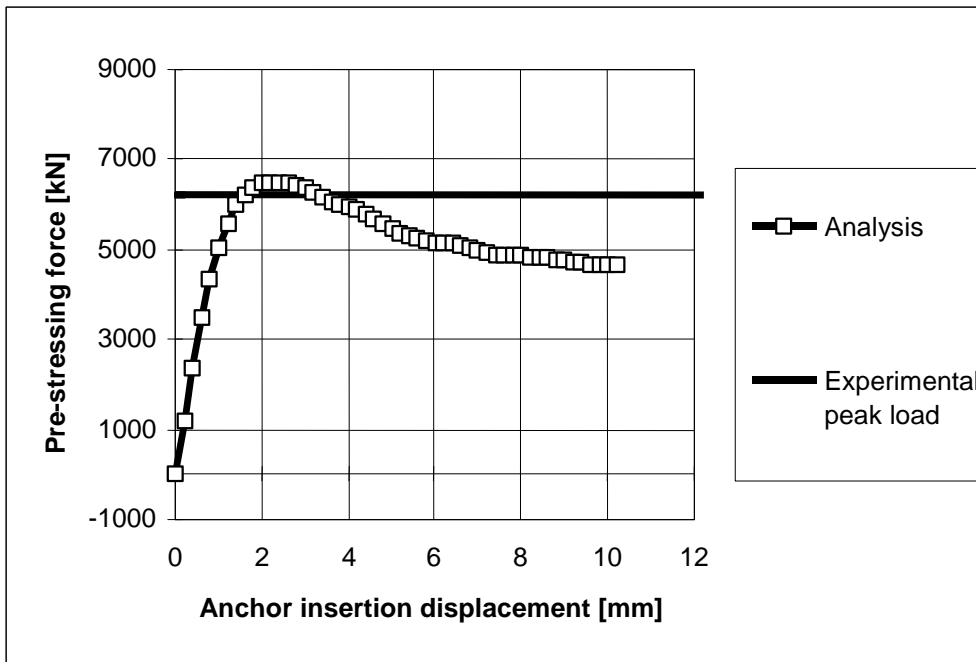


Fig. 17. Load-displacement diagram for pre-stressing anchor analysis.

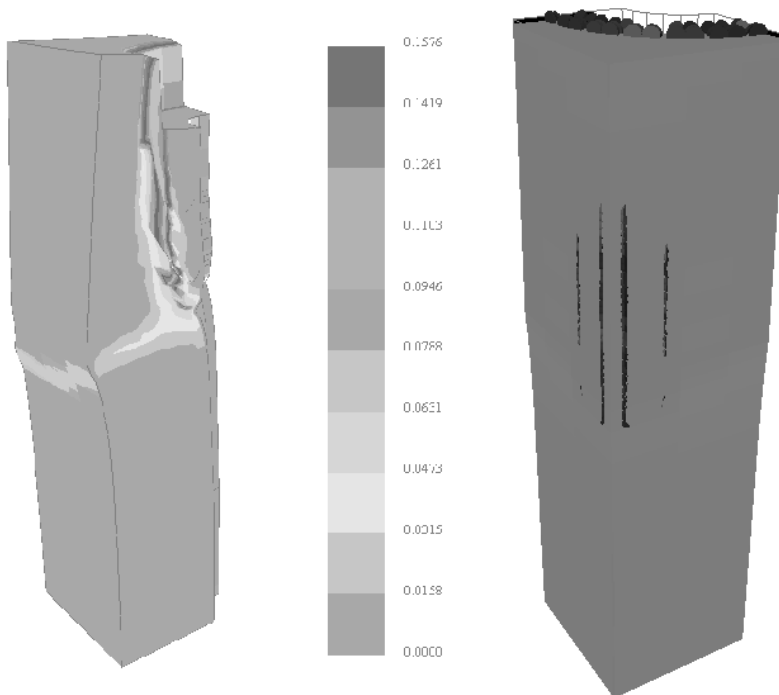


Fig. 18. Final failure mode for pre-stressing cable anchor analysis. Crushed concrete is shown in the left figure as contours of maximal plastic strain. Major radial/splitting cracks on the specimen surface are shown in the right figure.

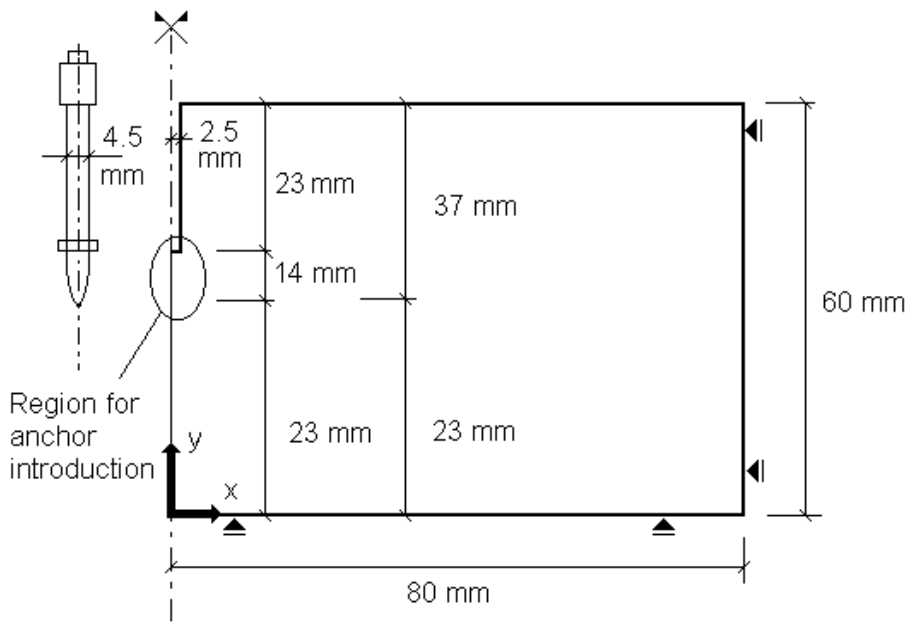


Fig. 19. Geometry of the specimen for testing of powder actuated anchors

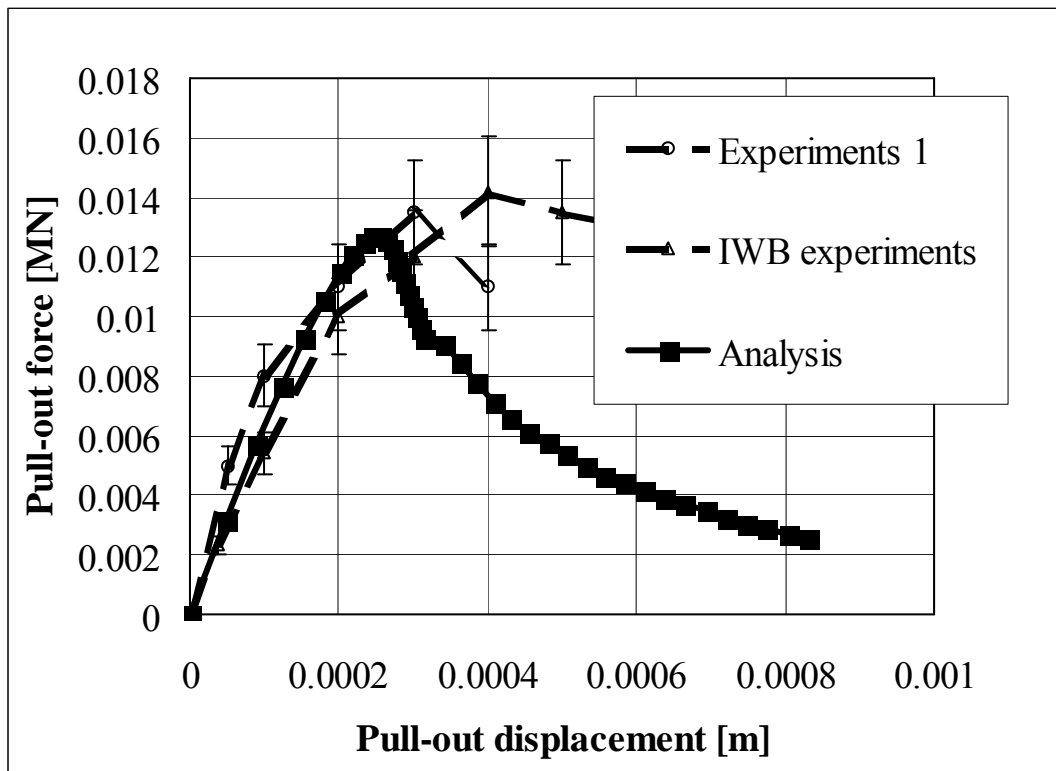


Fig. 20. Comparison of the finite element analysis with experimental data.

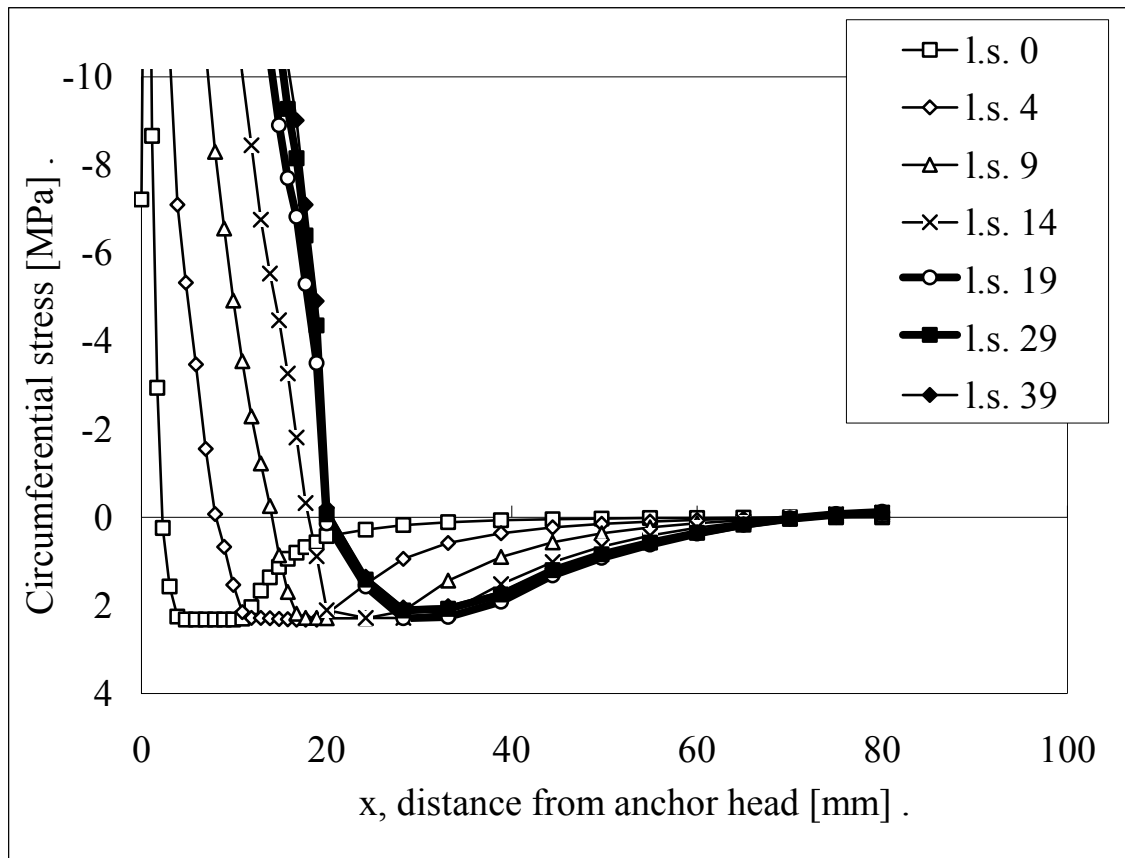


Fig. 21. Evolution of circumferential stresses around the anchor head showing the radial crack closure. Load step 19 is the end of insertion and load step 29 is at the peak pull-out force.

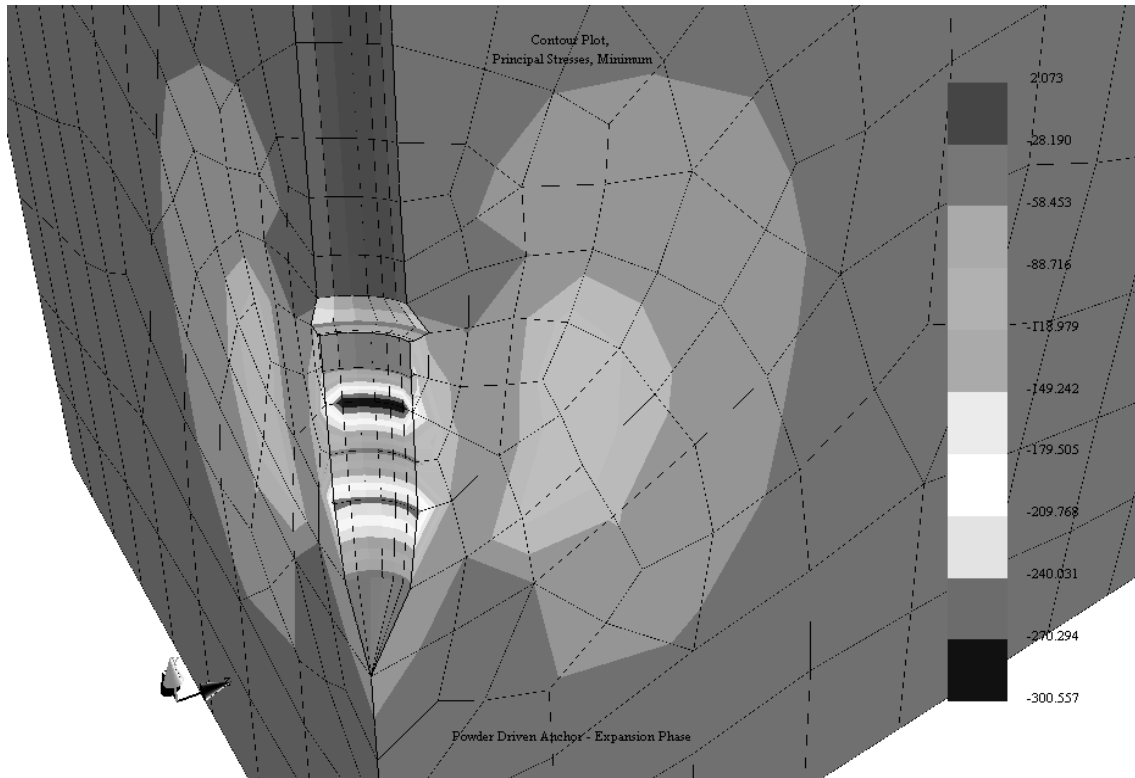


Fig. 22: Minimal principal stresses in the analysis at the end of expansion (i.e. insertion) phase.